Growth of plasma waves of scales longer than 10 km by gradient-drift instability in the E-region of equatorial ionosphere

E. A. Kherani, R. Bharuthram, and S. K. Maharaj

Growth of plasma waves of scales longer than 10 km by gradient-drift instability in the E-region of equatorial ionosphere

E. A. Kherani,[1,a)] R. Bharuthram,[2] and S. K. Maharaj[3]

[1]*Instituto Nacional de Pesquisas Espaciais (INPE), Av. dos Astronautas, São José dos Campos 12227010, Brazil*
[2]*University of the Western Cape (UWC), Robert Sobukwe Road, Bellville 7535, South Africa*
[3]*South African National Space Agency (SANSA) Space Science, P.O. Box 32, Hermanus 7200, South Africa*

In this study, a linear analysis of the Gradient Drift Instability (GDI) applicable for horizontal wavelengths longer than 10 km in the E region is presented. By analytically solving the non-local differential equation for the polarization potential, analytical forms of the dispersion relation and growth rate, hosting new contributions from non-local effects, are obtained. The new growth rate and the amplitude of polarization potential are examined for a wide range of wavelengths that reveal the positive growth of GDI for wavelengths of ∼25 km. These characteristics raise the possibility of the formation of unstable structures of vertical size ∼20–30 km in the upper E region, often observed during twilight hours. *Published by AIP Publishing.*
https://doi.org/10.1063/1.5034018

I. INTRODUCTION

The Gradient Drift instability (GDI) has been widely invoked to explain irregular density structures observed in the equatorial E region. Linear local/non-local theories of GDI[1–6] and numerical simulations[7,8] have been found to explain observations of meter to kilometer (small to intermediate to large) scale irregular structures.[3,6,9]

Thus far, theoretical/numerical studies have been restricted to the horizontal wavelengths of the perturbation (λ), less than 10 km. However, observations have found the presence of altitude-extended irregular structures attaining the vertical size of ∼20–30 km during twilight hours.[6] Interestingly, local GDI theories predict excitation of vertical size of ∼20–30 km by a large horizontal wavelength of ∼2 km.[6] Reference 6 argued the formation of ∼20–30 km structures in the E region, based on the tunneling mechanism in which two unstable regions, separated by the stable region, communicate to each other. In the present study, we aim to explore another mechanism that may directly excite the vertical size longer than 10 km, without relying on the tunneling mechanism. It is based on the fact that the vertical size of an unstable structure excited by GDI should be proportional to the horizontal wavelength of the perturbation.[3] Therefore, it is of interest to examine growth characteristics of GDI for horizontal wavelengths longer than 10 km that may give rise to vertical structures of comparable sizes.

In the present study, we refer to the wavelength range $10 \leq \lambda \leq 50$ km as the Large-to-Meso (LM) scale, since ranges $1 \leq \lambda \leq 10$ km and $\lambda \geq 100$ km are classified as large and meso-scales, respectively, in the literature. Obviously, for the LM scale, the local approximation breaks down, and therefore, non-local effects are required to be considered. The main focus of the present study is to investigate non-local growth of GDI for LM scales for which no report is available in the literature to date. Another objective of the study is to derive an analytical form of the growth rate for LM scales, similar to that derived by Kudeki *et al.*[3] and by Riggins and Kadish[4] for the intermediate and large scales. The aim of such reformulation is to accommodate scales from meters to LM in a unique growth rate expression so that it can be utilized to investigate the development of unstable structures of diverse nature in the E region.

This paper is organized as follows. In Sec. II, the non-local analysis of GDI is presented. In Sec. III, results are presented in which the derived analytical form of the polarization potential and the growth rate are examined for the realistic deserved E region conditions.

II. NON-LOCAL ANALYSIS

The starting point is the governing non-local differential equation for the polarization potential (φ) derived as Eq. (9) by Riggin and Kadish[4] which is written as follows:

$$\frac{d^2\varphi}{dy^2} + \frac{1}{L}\frac{d\varphi}{dy} + (R - k^2)\varphi = 0, \qquad (1)$$

where

$$R = i\frac{k}{L}\frac{\nu}{\Omega}\frac{(\omega + 2i\alpha n_o)}{(\omega - kv_d + 2i\alpha n_o)}.$$

Here, (y, L) represent the altitude and electron density scale height, (ω, k) represent the frequency and horizontally westward wavenumber of the perturbation, (n_o, v_d) represent the ambient density and horizontally westward drift of electrons relative to ions, and $(\alpha n_o, \nu, \Omega)$ represent the dissociative recombination rate, ion-neutral collision frequency and ion gyrofrequency, respectively. In writing R, the term $\frac{\nu\nu_e}{\Omega\Omega_e}$ is omitted compared to unity.

The above equation is derived in the Cartesian (x–y) plane perpendicular to the geomagnetic field, where ($\hat{x}$) and ($\hat{y}$) represent unit vectors in westward and upward directions,

a)esfhan.kherani@inpe.br

respectively. All ambient variations are considered in the (y) direction, i.e., the ionosphere is considered to be horizontally stratified. Initial perturbations $(\delta n, \delta E = -\nabla \varphi)$ are introduced for the ambient condition (n_o, E_o) such that $n = n_o + \delta n$, $E = E_o - \nabla \varphi$, where (φ) is the electrostatic potential. These perturbations are considered in the $(\hat{x})$ direction of the plane wave form $\delta(y) \exp (ikx - i\omega t)$, where (k, ω) are the perturbation wavenumber and frequency.

In obtaining Eq. (1), the following assumptions have been made by Riggin and Kadish: (i) Altitude variation of collision frequency (ν) is neglected in comparison to the altitude variation of the ambient electron density (n_o), (ii) altitude variation of v_d is neglected, (iii) pressure gradient force is not considered implying exclusion of diffusion effects on GDI, (iv) the perturbation is electrostatic in nature, and (v) $\frac{\nu}{\Omega} \frac{\nu_e}{\Omega_e} \ll 1$, where (ν_e, Ω_e) are the electron collision and gyro frequencies. In addition, the defining characteristics of the E region, i.e., $\nu \gg \Omega$, $\nu_e \ll \Omega_e$, and $\frac{\nu}{\Omega} \gg \frac{\nu_e}{\Omega_e}$ are imposed (Prolls, chapter 4).[10]

A. Analytical solution of Eq. (1)

We employ the method of variation of parameters, i.e., $\varphi = \varphi_p \varphi_v$, where φ_p is a particular solution of (1) and φ_v is a dimension-less function. With this substitution in (1), the following solution of φ_v is obtained:

$$\varphi_v = A \int \exp (-\theta) dy, \tag{2}$$

where

$$\theta = \int \left(\frac{2}{\varphi_p} \frac{d\varphi_p}{dy} + \frac{1}{L} \right) dy$$

and A is the constant of integration.

B. Particular solution of Eq. (1)

The particular solution (φ_p) is obtained by the method described by Panayotounakos and Zarmpoutis.[11] According to this method, a particular solution of a second order differential equation of the Liouville form can always be written in the form of the zero order Bessel function $J_o(p)$, where (p) is an explicit function of original independent variable (y). Panayotounakos and Zarmpoutis [Sec. II, Eqs. (2.14a) and (2.20a)][11] have shown that any second order differential equation is equivalent to the Bessel Differential equation of order (ν), i.e.,

$$\frac{d^2 f}{dy^2} + h(y) \frac{df}{dy} + r(y) f$$
$$= 0 \Longleftrightarrow p^2 \frac{d^2 f}{dp^2} + p \frac{df}{dp} + (p^2 - \nu^2) f = 0,$$

provided the coefficients (h, r) satisfy the following coupled differential equations:

$$h = \frac{1}{p} \frac{dp}{dy} - \frac{1}{dp/dy} \frac{d^2 p}{dy^2}, \quad r = \left(1 - \frac{\nu^2}{p^2} \right) \left(\frac{dp}{dy} \right)^2,$$

which can be solved analytically for $\nu = 0$, leading to the following analytical expression of $p(y)$:

$$p = \pm \frac{\sqrt{r}}{h + (1/2r)dr/dy},$$

and therefore, the particular solution of the 2nd order differential equation is written as follows:

$$f_p = J_o(p(y)).$$

It is a particular solution since we have set $\nu = 0$. From (1), we note that

$$h = \frac{1}{L}, \quad r = R - k^2,$$

and therefore,

$$\varphi_p = J_o(p), \tag{3}$$

where

$$p = \pm \frac{(R - k^2)^{1/2}}{\frac{1}{L} + \frac{1}{2(R - k^2)} \frac{d}{dy}(R - k^2)} \equiv \pm \frac{(R - k^2)^{1/2}}{\frac{1}{L} - \frac{R}{2(R - k^2)} \frac{1}{L} \frac{dL}{dy}}.$$

We note from Fig. 1 that for the typical E region density profile denoted by the blue curve, $\frac{1}{L} \frac{dL}{dy} \approx 0$ everywhere except in the vicinity of large $L \to \infty$ where the local condition $(kL \gg 1)$ is unconditionally satisfied for all wavelengths. In other words, $\frac{1}{L} \frac{dL}{dy} \approx 0$ is a valid approximation under the non-local condition $(kL \ll 1)$ so that the term $-\frac{1}{2} \frac{R}{R-k^2} \frac{dL}{dy} \ll 1$ in the denominator is neglected. Thus, p can be simplified to the following form:
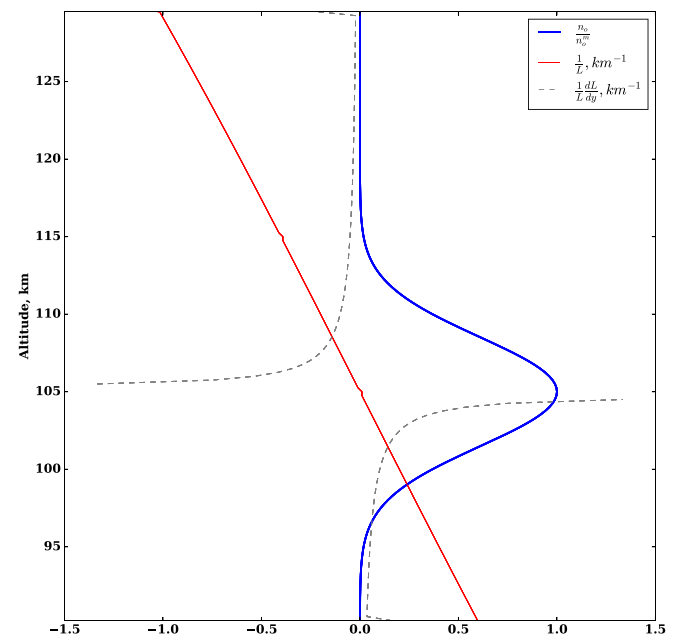
$$p = \pm L(R - k^2)^{1/2} \tag{4}$$

FIG. 1. Altitude variations of ambient electron density n_o, $\frac{1}{L} = \frac{1}{n_o} \frac{dn_o}{dy}$, and $\frac{1}{L} \frac{dL}{dy}$ are plotted. $n_o^m = 10^{10} m^{-3}$ represents the maximum value of n_o.

C. New dispersion relation

We note that $p = 0$ in Eq. (4) leads to the known dispersion relation derived by Kudeki et al.,[3] i.e.,

$$(\omega + 2i\alpha n_o)\left(1 - \frac{i}{kL}\frac{\nu}{\Omega}\right) = kv_d.$$

Therefore, Eq. (4) is the new non-local Dispersion relation, i.e.,

$$R - k^2 = \frac{p^2}{L^2}$$

or

$$\frac{i}{kL}\frac{\nu}{\Omega}\frac{(\omega + 2i\alpha n_o)}{(\omega - kv_d + 2i\alpha n_o)} - 1 = \frac{p^2}{k^2 L^2} \equiv \frac{-\Lambda}{k^2}. \quad (5)$$

Here, Λ is the eigen value of Eq. (1) since the equation can be written as $M\varphi = -(R - k^2)\varphi \equiv \Lambda\varphi$, where M is the differential operator in (1). Considering $\omega = \omega_r + i\gamma$ in (5), the following frequency and growth rate expressions of the GDI are obtained:

$$\omega_r = \frac{kv_d}{1 + \eta_\Lambda^2}; \quad \gamma = -2\alpha n_o + \gamma_{\text{new}}; \quad \gamma_{\text{new}} = \frac{\eta_\Lambda}{1 + \eta_\Lambda^2}kv_d, \quad (6)$$

where

$$\eta_\Lambda = \frac{\eta}{1 - \Lambda/k^2}; \quad \eta = \frac{i}{kL}\frac{\nu}{\Omega}. \quad (7)$$

We note that, in the limit $\Lambda/k^2 \ll 1$, the growth rate (γ_o) derived by Kudeki et al.[3] is retrieved from (6), i.e.,

$$\omega_o = \frac{kv_d}{1 + \eta^2}; \quad \gamma_o = \frac{\eta}{1 + \eta^2}kv_d. \quad (8)$$

D. Analytical expression for the eigenmodes

From (2) and (3), we note that the polarization potential, $\varphi = J_o(p)\varphi_v(p)$, depends on p which is proportional to Λ. Therefore, φ are the eigenmodes, corresponding to the eigen values Λ. The exponent θ in φ_v in (2) is estimated as follows:

$$\varphi_v = A\int dy \exp\left[-\int\left(\frac{2}{\varphi_p}\frac{d\varphi_p}{dy} + \frac{1}{L}\right)dy\right].$$

Here

$$\frac{d\varphi_p}{dy} = \frac{d\varphi_p}{dp}\frac{dp}{dy} = -J_1(p)\frac{dp}{dy}$$

and

$$\frac{dp}{dy} = \pm\frac{d}{dy}(L(R - k^2)^{1/2})$$

or

$$\frac{dp}{dy} = (R - k^2)^{1/2}\frac{dL}{dy} + \frac{1}{2(R - k^2)}\frac{dR}{dy}$$

$$\equiv (R - k^2)^{1/2}\frac{dL}{dy} - \frac{R}{2(R - k^2)^{1/2}}\frac{dL}{dy},$$

where only the derivative of L is retained in estimating dR/dy. Finally, we have

$$\frac{dp}{dy} = \frac{1}{2}\frac{(R - 2k^2)}{(R - k^2)^{1/2}}\frac{dL}{dy} \equiv \frac{1}{2}\left(1 - \frac{k^2 L^2}{p^2}\right)\frac{p}{L}\frac{dL}{dy}.$$

Therefore

$$\frac{1}{\varphi_p}\frac{d\varphi_p}{dy} + \frac{1}{L} = -\frac{J_1}{2J_o}\left(1 - \frac{k^2 L^2}{p^2}\right)\frac{p}{L}\frac{dL}{dy} + \frac{1}{L}.$$

Since $\frac{1}{L}\frac{dL}{dy} \approx 0$ under the non-local condition and $p = 0$ for the local condition, as argued in Subsection II C, the first term in the right hand side can be neglected. Thus, the following simplified expression for θ is obtained:

$$\theta = \int\frac{1}{L}dy \equiv \log(n_o).$$

In order to evaluate the integral in (2), the altitude variation of electron density of the following Gaussian form is considered:

$$n_o(y) = N\exp\left(-(y - y_o)^2/\sigma^2\right)m^{-3}, \quad (9)$$

where (N, y_o, σ) are constants. Thus, φ_v from (2) is obtained as follows:

$$\varphi_v = A\int dy\exp(-\log n_o)$$

$$\equiv A\exp(-\log N)\int dy\exp\left[\frac{(y - y_o)^2}{\sigma^2}\right]$$

and, the eigenmode $(\varphi = \varphi_p\varphi_v)$ can be written as follows:

$$\varphi = BJ_o(p)\int dy\exp\left(\frac{(y - y_o)^2}{\sigma^2}\right), \quad (10)$$

where $\varphi_p = J_o(p)$ from (3) is used and B absorbs all the constants. The solution (10) is further reduced to the following form:

$$\varphi = (\sqrt{\pi}B)J_o(p)\mathcal{E}\text{rfi}\left(\frac{y - y_o}{\sigma}\right), \quad (11)$$

where $\mathcal{E}\text{rfi}$ is the imaginary error function. The expression (11) is the exact solution of (1) and is examined under realistic E region conditions in Sec. III. It is to be solved numerically owing to the presence of the error function. However, much of insight of the solution can be inferred by examining (10) under valid approximations, namely, the thin E layer assumption. On such a condition, $(y - y_o)^2$ can be approximated to $|y - y_o|\sigma$ since σ and $(y - y_o)$, i.e., width and total extent of layer, are of the same order. Thus

$$\varphi_{\text{ana}} \approx (\sqrt{\pi}B)J_o(p)\int dy\exp\left(\frac{|y - y_o|}{\sigma}\right)$$

or

$$\varphi_{\text{ana}} = (\sqrt{\pi}B\sigma)J_o(p)\exp\left(\frac{|y - y_o|}{\sigma}\right). \quad (12)$$

Therefore, the eigenmodes possess both oscillatory and exponential variations with the altitude, suggesting their unstable and non-local nature.

E. Estimation of *p*

We note from (5) and (6) that the estimation of *p* requires *a priori* knowledge of $\omega = \omega_r + i\gamma$ that itself depends on *p*. These coupled algebraic equations are solved by the Predictor-Corrector method as follows: In (5), *p* is predicted by substituting $\omega = \omega_o$ from (8) and then ω is predicted from (6). In the correction mode, *p* is corrected by substituting predicted ω in (5) and subsequent corrected ω is obtained for the corrected *p*. This correction mode is repeated until the convergence of two consecutive corrected *p* occurs.

III. RESULTS AND DISCUSSION

Expressions (6), (11), and (12) are examined in the E region between 90 km and 130 km altitude under typical ambient night-time conditions (Prolls, chap. 4)

$$n_o = 10^{10} \exp\left(-(y-105)^2/10^2\right) m^{-3}, \quad \alpha = 10^{-13} m^3/s,$$

$$\frac{\nu}{\Omega} = 10^2 \exp\left(-(y-90)/15\right), \quad v_d = -100 m/s. \qquad (13)$$

Note that v_d is negative since electron drifts eastward during night-time. Altitude variations of the equilibrium electron density (n_o) and the corresponding inverse of scale height ($1/L$) are shown in Fig. 1. In Fig. 2, altitude variations of growth rates (γ_{new}, γ_o) of GDI, as given by Eqs. (6) and (8), are plotted. In Fig. 3, the altitude variation of eigenmode (φ) given by Eq. (11) is plotted. Six panels in Figs. 2 and 3 correspond to six values of horizontal wavelength of perturbation ($\lambda = 2\pi/k$), as indicated at the top of each panel, representing small scales ($\lambda = 400$ m), intermediate scale ($\lambda = 1$ km), large scale ($\lambda = 5$ km), large-to-meso (LM) scale ($\lambda = 25$ km), and meso scale ($\lambda = 125$ km). Though, for LM scales, γ_o is not applicable, they are still plotted for LM and meso scales in Fig. 2 for the comparative study. In Fig. 3, (φ_{ana}, φ_p), i.e., the analytically approximate eigenmode, as given by (12), and the particular solution, as given by (3), are also plotted.

From Fig. 2, we note that for $\lambda \leq 1$ km, both (γ_{new}, γ_o) are the same, as expected. Moreover, they are positive in the upper E region as expected during night-time. On the other hand, for $\lambda \geq 5$ km, γ_{new} departs significantly from γ_o though
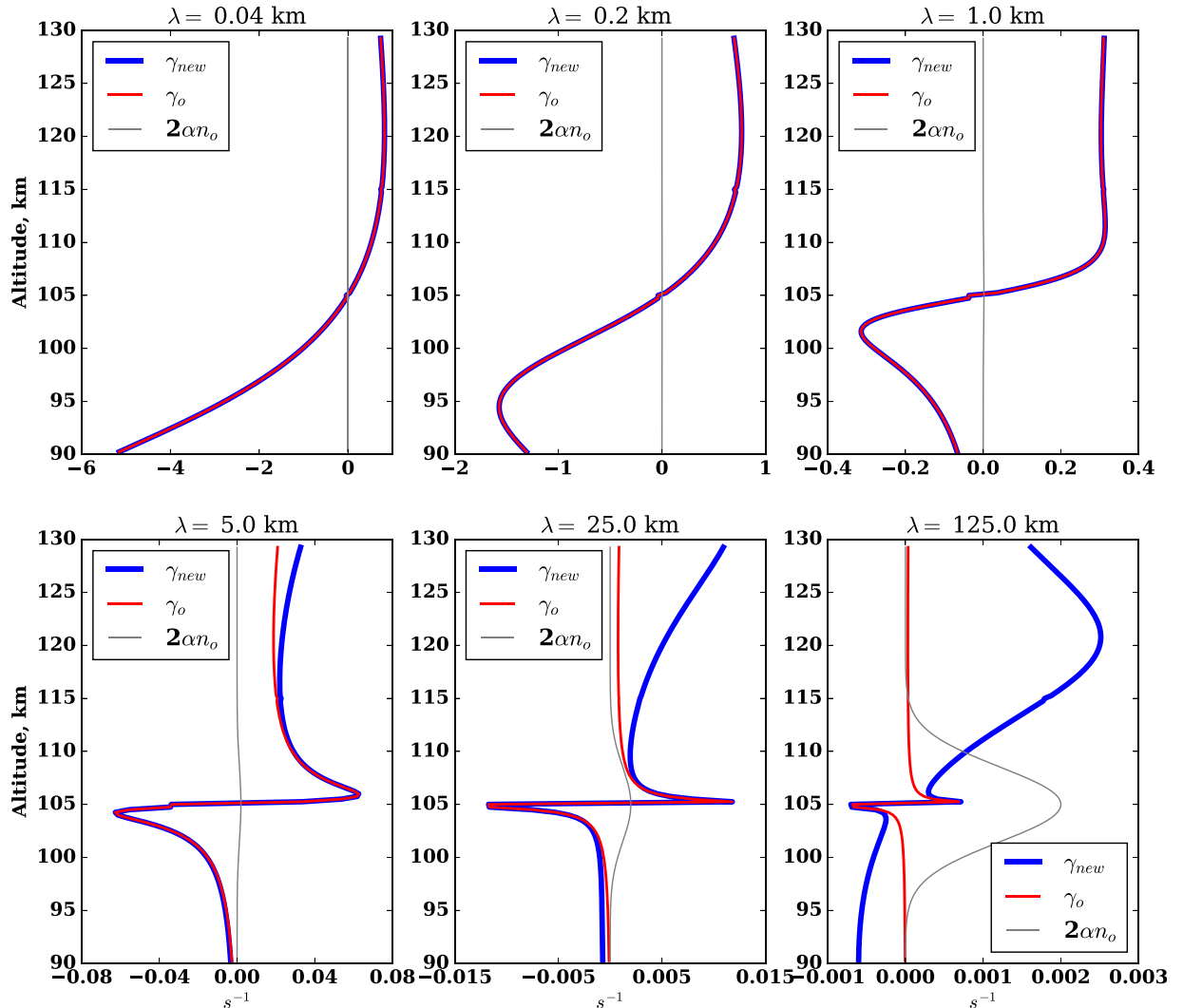

FIG. 2. Altitude variation of the new growth rate (γ_{new}) given in (6) and the growth rate (γ_o) derived by Kudeki *et al.*[3] and given in (8). Six panels correspond to six values of horizontal wavelength of perturbation λ indicated at the top of each panel. The recombination damping rate ($2\alpha n_o$) is also plotted. These results are obtained by considering the eastward drift $v_d = -100$ m/s.

both remain positive in the upper E region. Exceptionally, they are identical in the narrow altitude region around 105 km, where $L \to \infty$, and thus the condition $kL \gg 1$, i.e., $\Lambda/k^2 \ll 1$, is unconditionally satisfied for all wavelengths, reducing γ_{new} to γ_o.

We note that γ_{new} decreases with increasing λ such that the growth of LM scales (e.g., $\lambda = 25$ km) is an order slower than the growth of large scales (e.g., $\lambda = 5$ km) and even much slower than intermediate (e.g., $\lambda = 1$ km) and small scales (e.g., $\lambda = 400$ m). However, the growth rate of the LM scale remains larger than the recombination rate in the entire upper E region, as we note for the LM scale. For the meso scale ($\lambda = 125$ km), we note that the growth rate and recombination rate begin to overlap in altitudes, suggesting insignificant growth of such scales in the E region.

In Fig. 3, we note that the amplitude of eigenmode (φ) increases with λ which is expected for any convective instability such as GDI.[3] Under convective instability, longer wavelengths grow slower than the shorter wavelengths, as also noted in Fig. 2. It means that the longer wavelength modes are much more amplified in comparison to the

shorter wavelengths since they have sufficient time to accumulate free energy. This aspect is consistently reflected in Fig. 3. Another consistent aspect in Fig. 3 is that the eigenmodes attain maximum (minimum) in the small (large) L region, i.e., in strong (weak) density gradient regions. This aspect is expected for instability driven by the density gradient, as in the present case. It also implies that the eigenmodes are bounded and unstable since they are attenuated while propagating and therefore have favorable conditions to accumulate free energy in the localized altitude region. We also note that these eigenmodes acquire vertical variation scales proportional to the corresponding horizontal wavelengths, i.e., the horizontal wavelengths are consistently reflected in the vertical variations of the eigenmodes. Note that λ enters though (p), given by (5), and the eigenmode is the function of p through $\varphi_p = J_o(p)$. Therefore, the consistent reflection of wavelength in eigenmodes ensures the proper estimation of (p) by the predictor-corrector method. It also reflects the robust nature of the analytical procedure adopted in the present study, to solve the non-local differential equation (1).
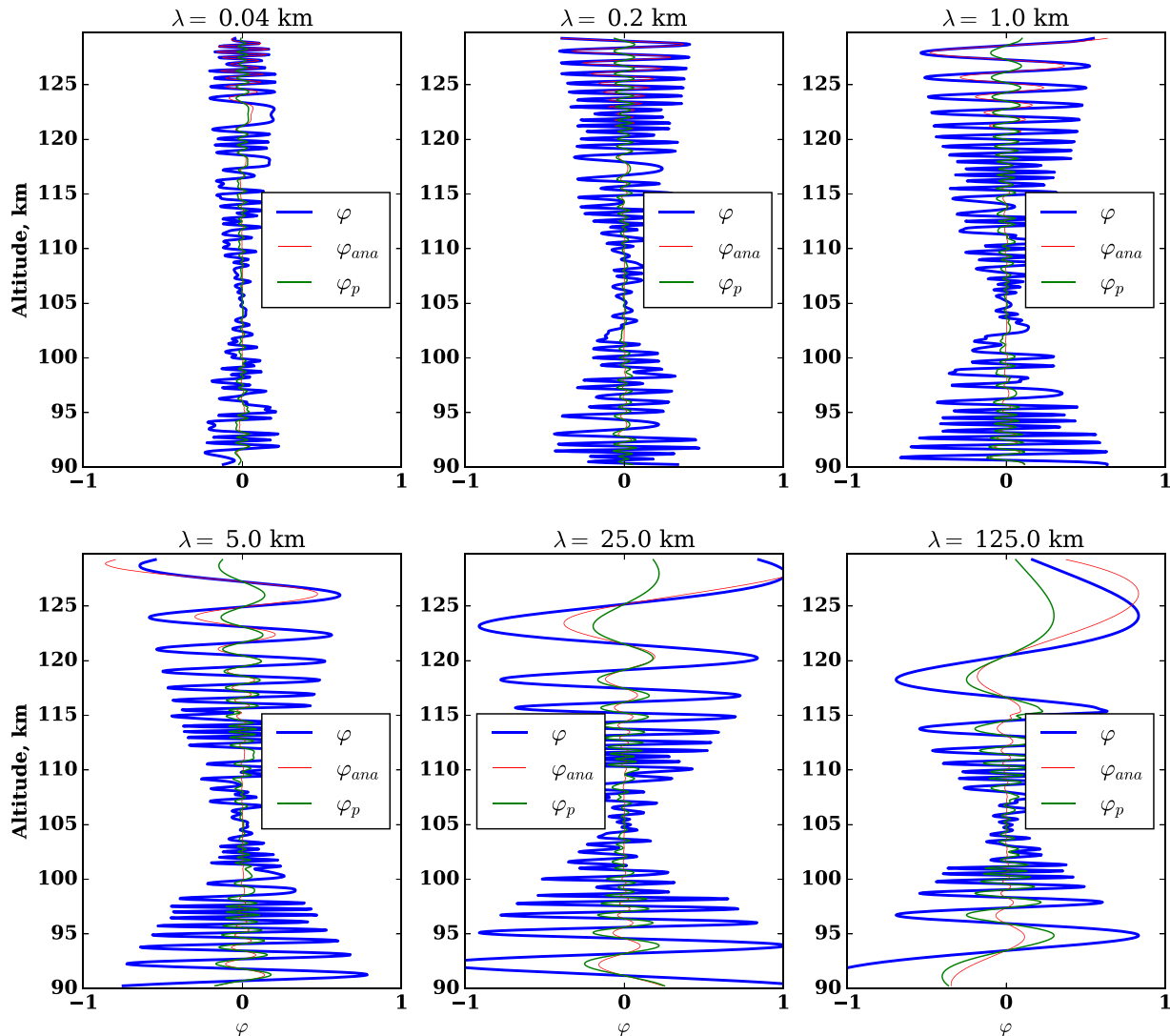

FIG. 3. Altitude variation of eigenmode or potential (φ) derived as expression (11). Six panels correspond to six values of horizontal wavelength of perturbation as indicated at the top of each panel. The analytical approximate eigen mode (φ_{ana}) given by (12) and the particular solution (φ_p) given by (3) are also plotted. All these potentials are normalized to the constant (B).

We also note that φ has a similar altitude variation to φ_p and the presence of an exponential factor in (8) does not alter the variation significantly. Therefore, the particular solution of (1) itself provides a glimpse of the eigenmode and much of the eigenmode features can be inferred without estimating the complex integrals in (2). Interestingly, the numerical solution (φ) and the analytical solution (φ_{ana}) have a similar altitude variation though they differ in the amplitude. The similarity suggests that the major variation stems from φ_p, which is kept the same in both φ and φ_{ana}.

During twilight hours, the ambient E region departs from the single layer structure and becomes composed of multiple sub-layers (Ronchi *et al.*).[7] We aim to examine the present non-local analysis for such a twilight scenario, for which ambient (n_o) is considered of the following form:

$$n_o(y) = 10^{10} \exp\left(-(y-105)^2/10^2\right) + 5$$
$$\times\, 10^9 \exp\left(-(y-115)^2/10^2\right) \mathrm{m}^{-3}. \quad (14)$$

Other ambient conditions remain unchanged from (13). Results for the twilight scenario and for $\lambda = 25$ km are presented in Fig. 4. We note two altitude regions of positive growth as expected. The growth and eigenmode attain maximum in the upper layer in the 115–130 km altitude region. The phase velocity in 4(D) also maximizes in this altitude region. Interestingly, the wave propagates with the velocity

much smaller than the electron drift, an aspect also known for the large scale GDI.[3]

Therefore, LM scales are preferably excited in 115–130 km altitudes during twilight. It is to be mentioned that a majority of twilight irregular structures of vertical size $\sim$25 km are observed in this altitude region.[6] Therefore, the present study consistently explains their presence in the upper E region. The past non-local studies were confined to the longer scales and successfully interpreted the presence of altitude extended structures of size less than 10 km that were reported in various observations.[3,6,7] Also, a local analysis finds that even for the long horizontal wavelength of $\sim$2 km, the growth rate can be positive for the vertical wavelength of $\sim$20 km.[6] Evidently, the present study accommodates these aspects of longer scales as well as brings out new aspects about the growth of LM scales.

The eigenmode φ in Figs. 3 and 4 tends to increase at the upper and lower boundaries. This behavior is due to the $n_o(y)$ profile that has corresponding L decreasing towards the boundaries. In order to understand the sensitivity of the $n_o(y)$ profile upon the eigenmode, the analysis is carried out below by considering the following profile:

$$n_o = 10^{10} \exp\left(-(y-110)^2/10^2\right)$$
$$+ 10^9 \left(1 + \epsilon\, \frac{\tanh[4\pi(y-140)/l_w]}{1-\epsilon}\right) \mathrm{m}^{-3}. \quad (15)$$
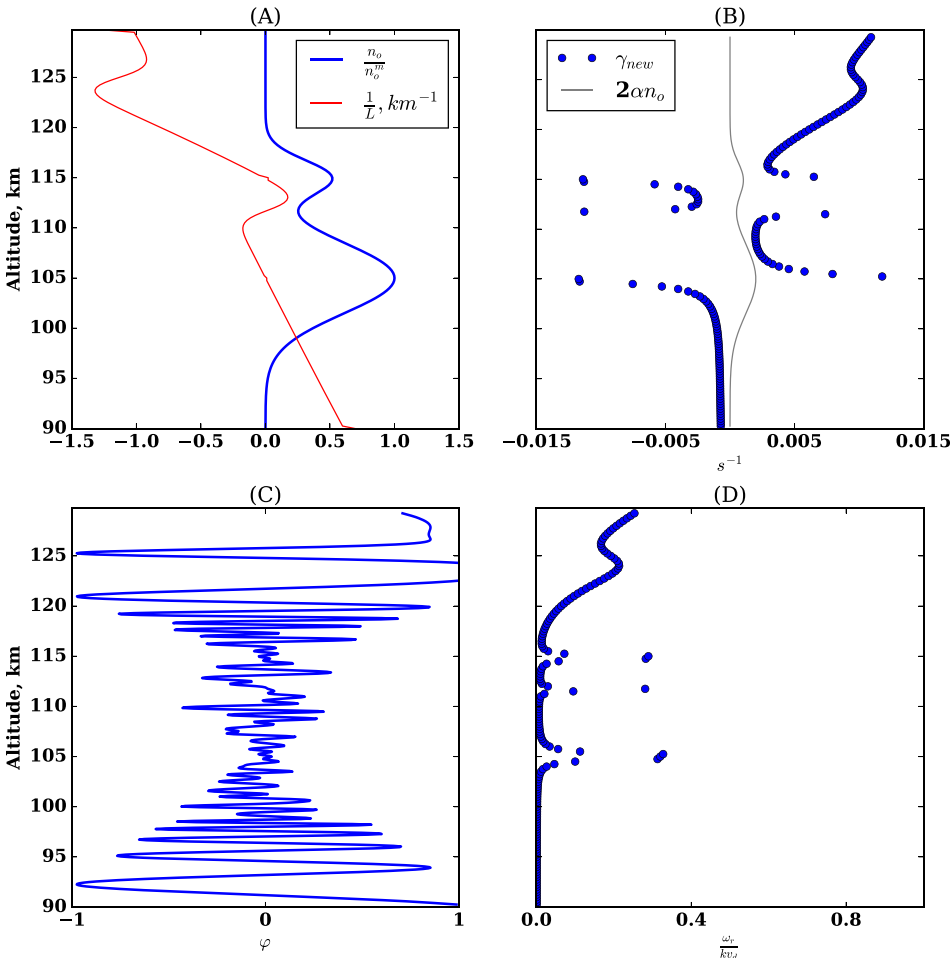

FIG. 4. Twilight scenario: Altitude variations of (a) n_o and L, (b) γ_{new} and recombination damping rate, (c) eigenmode φ and (d) phase velocity ω_r/k, normalized to $v_d = -100$ m/s.
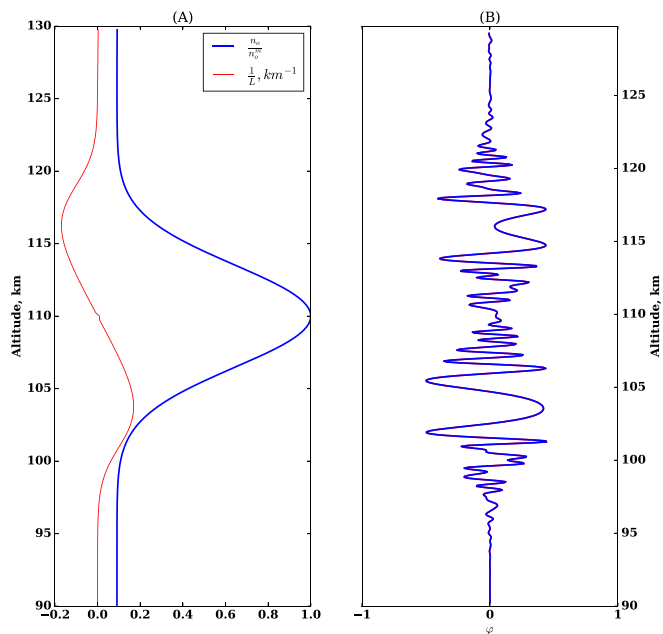
FIG. 5. Case corresponding to the profile (15): Altitude variations of (a) n_o and L, (b) eigenmode φ.

The second segment in n_o is similar to that considered by Huba and Lee[2] with $\epsilon = 0.8$ which is retained in the present study. In (15), $l_w = 40$ km is the thickness of the E layer. The resultant density profile is shown in Fig. 5(a). We note that unlike the previous profiles in Figs. 1 and 4(a), the present profile has corresponding L increasing towards the boundaries. The associated eigenmode φ is shown in Fig. 5(b). We note that unlike in Figs. 3(d)–4(c), the eigenmode in the present case in Fig. 5(b) decreases towards the boundaries, demonstrating the consistent behavior in response to the scale height L and sensitivity to the $n_o(y)$ profile.

IV. SUMMARY

This study reformulates the non-local linear analysis of GDI in the E region of equatorial ionosphere with the aim to study the growth of horizontal perturbation of wavelengths longer than 10 km which we have referred as Large-to-Meso (LM) scales. For such scales, growth characteristics remain unexplored to date. The non-local differential equation for the polarization potential derived by Riggin and Kadish[4] is solved under conditions where the altitude variation of the electron density scale height is retained. Its solution is obtained analytically and found to be proportional to the zero-order Bessel function whose argument leads to the analytical form of the dispersion relation with the new non-local term associated with the eigen value. The eigenmodes and their growth are examined under night-time and twilight E region conditions. The new growth rate reproduces the same results for meter to long wavelengths, as known from the previous studies, i.e., their growths are much larger than the recombination damping.

New results are as follows: (1) For LM wavelengths of ~ 25 km, the new growth rate is found to be larger than the damping rate, though they grow slower than the long scales and even much slower than the intermediate and small scales, (2) corresponding eigenmode acquires large amplitude in the strong density gradient region revealing its bounded and unstable nature, (3) its amplitude is comparable to that of longer scale and even larger than that of intermediate/small scales, (4) it is sensitive to the chosen density profile, (5) it propagates with the phase velocity much smaller the electron drift velocity. Therefore, horizontal perturbation of LM scales can grow in the E region, raising the possibility of the formation of unstable structures of similar vertical scales which are often observed in the twilight-evening time upper E region.

[1]R. N. Sudan, J. Akinrimisi, and D. T. Farley, "Generation of small-scale irregularities in the equatorial electrojet," J. Geophys. Res. **78**, 240, https://doi.org/10.1029/JA078i001p00240 (1973).

[2]J. Huba and L. Lee, "Short wavelength stabilization of the gradient drift instability due to velocity shear," Geophys. Res. Lett. **10**(4), 357–360, https://doi.org/10.1029/GL010i004p00357 (1983).

[3]E. Kudeki, D. T. Farley, and B. G. Fejer, "Long wavelength irregularities in the equatorial electrojet," Geophys. Res. Lett. **9**, 684, https://doi.org/10.1029/GL009i006p00684 (1982).

[4]D. Riggin and A. Kadish, "Nonlocal theory of long-wavelength plasma waves associated with sporadic E layer," J. Geophys. Res. **94**, 1495–1500, https://doi.org/10.1029/JA094iA02p01495 (1989).

[5]C. Ronchi, P. Similon, and R. Sudan, "A nonlocal linear theory of the gradient drift instability in the equatorial electrojet," J. Geophys. Res. **94**(A2), 1317–1326, https://doi.org/10.1029/JA094iA02p01317 (1989).

[6]D. L. Hysell and J. L. Chau, "Imaging radar observations and non-local theory of large scale plasma waves in the equatorial electrojet," Ann. Geophys. **20**, 1167–1179 (2002).

[7]C. Ronchi, R. N. Sudan, and D. T. Farley, "Numerical simulations of large-scale plasma turbulence in the daytime equatorial electrojet," J. Geophys. Res. **96**, 21263, https://doi.org/10.1029/91JA01951 (1991).

[8]S. Hu and A. Bhattacharjee, "Gradient drift instabilities and turbulence in the nighttime equatorial electrojet," J. Geophys. Res. **104**, 28123, https://doi.org/10.1029/1999JA900399 (1999).

[9]A. K. Patra and P. B. Rao, "High-resolution radar measurements of turbulent structure in the low-latitude E region," J. Geophys. Res. **104**, 24667, https://doi.org/10.1029/1999JA900303 (1999).

[10]G. Prolls, *Physics of the Earth's Space Environment* (Springer-Verlag Berlin Heidelberg, 2004).

[11]D. E. Panayotounakos and T. I. Zarmpoutis, "Construction of exact parametric or closed form solutions of some unsolvable classes of nonlinear ODEs (Abel's Nonlinear ODEs of the first kind and relative degenerate equations)," Int. J. Math. Math. Sci. **2011**, 1–13..